# Shape-Dependent Cellular Processing of Polyelectrolyte Capsules

**Olga Shimoni,‡ Yan Yan,‡ Yajun Wang, and Frank Caruso***

Department of Chemical and Biomolecular Engineering, The University of Melbourne, Parkville, Victoria 3010, Australia. ‡These authors contributed equally.

**ABSTRACT** Particle shape is emerging as a key design parameter for tailoring the interactions between particles and cells. Herein, we report the preparation of rod-shaped layer-by-layer (LbL)-assembled polymer hydrogel capsules with tunable aspect ratios (ARs). By templating spherical and rodlike silica particles, disulfide-stabilized poly(methacrylic acid) hydrogel capsules (PMA HCs) with different ARs (from 1 to 4) are generated. The influence of capsule AR on cellular internalization and intracellular fate was quantitatively investigated by flow cytometry, imaging flow cytometry, and fluorescence deconvolution microscopy. These experiments reveal that the cellular internalization kinetics of PMA HCs are dependent on the AR, with spherical capsules being internalized more rapidly and to a greater extent compared with rod-shaped capsules. In contrast, the capsules with different ARs are colocalized with the lysosomal marker LAMP1, suggesting that the lysosomal compartmentalization is independent of shape for these soft polymer capsules.

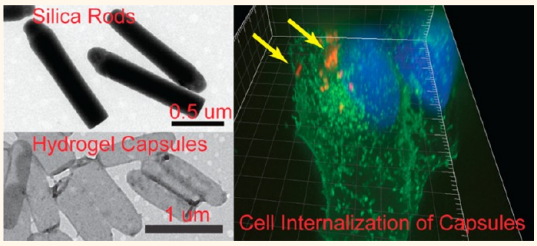


**KEYWORDS:** aspect ratio · cell internalization · intracellular fate · polyelectrolyte capsules · layer-by-layer assembly

In the past few decades a suite of drug carrier systems, including liposomes,[1] polymersomes,[2] micelles,[3] and polymer capsules[4,5] have been developed to improve the specificity and efficacy of drugs. Advances in this field are dependent on, among other factors, the physicochemical properties of particles, including size, shape and surface chemistry.[6,7] Hence, controlling such properties is an active area of research. For example, surface functionalization with antifouling (*e.g.*, poly(ethylene glycol))[8] and/or targeting molecules (*e.g.*, antibodies)[9] has been widely explored to enhance the specificity of particles. In addition to a range of chemistry-derived solutions for improving particle characteristics, the development of fabrication techniques that are capable of generating particles with well-controlled physical properties (*e.g.*, size, shape, and rigidity) have emerged as novel approaches to control the biological behavior of particles.[10,11]

In particular, the aspect ratio (AR) of particles is recognized as an important particle design parameter. Tuning the AR can lead to improved biodistribution[12,13] and tumor penetration of particles.[14] Given the importance of cellular uptake in effective drug delivery, the influence of shape on internalization has also been observed for several particle systems. However, varied results have been reported regarding the impact of AR on cellular interactions for different particles. For example, spherical gold nanoparticles are internalized to a greater extent than gold nanorods with higher ARs [AR $\approx$ 3 (14 $\times$ 40 nm) and AR $\approx$ 5 (14 $\times$ 74 nm)].[15] Consistent with this observation, spherical poly(lactide-*co*-glycolide) microparticles are internalized more rapidly than elliptical particles with the same internal volume, resulting in up to a 4-fold enhancement in the number of internalized spheres than elliptical particles.[16] In contrast, mesoporous silica rods with an AR of ~2.5 (60−90 nm $\times$ 160−190 nm) are internalized in cells in larger quantities compared with particles of similar composition and with AR $\approx$ 1.5 (60−80 nm $\times$ 110−130 nm) or AR $\approx$ 4.5 (50−70 nm $\times$ 260−300 nm).[17] Further, cationic poly(ethylene glycol)-based PRINT (particle replication in non-wetting templates) particles with AR $\approx$ 3 (150 $\times$ 450 nm) are internalized more efficiently and to a higher extent than spherical particles (200 nm).[18] The different effects on cellular uptake observed in these studies is, in addition to the particle AR, likely due to the various cellular endocytic pathways operating in response to the different composition of the particles. This highlights the complex interplay

* Address correspondence to fcaruso@unimelb.edu.au.

Received for review October 4, 2012 and accepted November 29, 2012.

**Published online December 12, 2012**
**10.1021/nn3046117**

**TABLE 1. Silica Template and PMA HC Sizes, Acquired from TEM Images[a]**

| | silica rod | | | capsule | | |
|---|---|---|---|---|---|---|
| | length, nm | width, nm | AR | length, nm | width, nm | AR |
| AR1 | 296 ± 20 | | 1.0 | 390 ± 40 | | 1.0 |
| AR2 | 430 ± 50 | 180 ± 40 | 2.4 | 700 ± 80 | 360 ± 60 | 1.9 |
| AR3 | 480 ± 40 | 160 ± 30 | 3.1 | 1120 ± 130 | 410 ± 65 | 2.7 |
| AR4 | 750 ± 140 | 185 ± 10 | 4.0 | 1290 ± 140 | 340 ± 60 | 3.8 |

[a] At least 100 particles/capsules were examined.

between particle shape and other physicochemical properties in governing cellular interactions.

Nanoengineered polymer capsules prepared by the layer-by-layer (LbL) technique are prominent candidates for drug delivery.[19,20] The versatility of LbL assembly allows the preparation of hollow polymer capsules of different shapes by templating various particles, including organic or inorganic spheres,[19,20] carbon or nickel nanotubes,[21,22] glass or electrospun polymer fibers,[23,24] bacteria,[25] red blood cells,[26] enzyme crystals,[27] or liquid crystal emulsions.[28] Despite the adaptability of LbL assembly, to our knowledge, there are no reports on the preparation of LbL polymer capsules with tunable ARs.

Poly(methacrylic acid) hydrogel capsules (PMA HCs) generated through LbL assembly and stabilized with disulfide linkages have been shown to possess high colloidal stability, efficient cargo encapsulation, triggered drug release,[29] and cancer cell targeting,[30] offering significant potential in advanced drug delivery. Recent progress has been made toward understanding the complex cellular interactions of spherical PMA HCs. It has been shown that such capsules can be readily internalized by a range of cells, including epithelial cells,[31] dendritic cells,[32] and monocytes.[32] Exofacial thiols on the cell membrane have been suggested to mediate their cellular interaction and cargo release.[33] Currently there are no reports on the preparation and cellular interactions of nonspherical PMA HCs. Given the increasingly recognized role of shape on cellular interaction and cellular dynamics, understanding the cellular behavior of PMA HCs with engineered AR is of particular importance for further development and optimization of these systems.

Herein, we report the first study on the fabrication of PMA HCs with different ARs. A series of silica particles with various ARs (from AR1 to AR4, see Table 1) were used as templates for LbL assembly. We demonstrate that the ultrathin hollow PMA HCs generated *via* LbL assembly retain similar ARs to their templates. Further, we investigate the influence of AR of the PMA HCs on cellular internalization dynamics and intracellular fate. It is shown that an increase in AR decreases the internalization efficiency of the capsules, but regardless of shape, the internalized PMA HCs are located in lysosomes. Given the versatility of LbL assembly, this study demonstrates the feasibility of using the LbL technique to generate a spectrum of polymer carriers with controlled shape and provides insights into the influence of PMA HC shape on biological interactions.

## RESULTS AND DISCUSSION

The size and shape of a series of PMA HCs were examined by TEM (Figure 1). The capsules retained the original shape of the templates and had similar ARs to the template silica particles; however, the dimensions were approximately two times larger than the templates (see Supporting Information, Figure S1). This is likely due to the hydrogel nature of the capsules, which causes them to swell in aqueous conditions, leading to larger sizes.[34] The capsule morphology, examined by AFM (Figure 2), shows that the capsules exhibit granular surfaces without folding. Measurement of the capsule height along the short and long axes by AFM for eight-layer PMA HCs showed relatively homogeneous profiles with an average thickness of 24 ± 3 nm, corresponding to 3 nm per layer (Supporting Information, Figure S2), which is consistent with the thickness of PMA layers in thin films measured by dual polarization interferometry.[35]

Next, we sought to investigate the role of capsule geometry on cellular uptake. HeLa cells were incubated with AF633-labeled PMA capsules at a capsule-to-cell ratio of 100:1, and the cellular association was evaluated by flow cytometry as a function of time. The cellular interaction of the capsules was a time-dependent process for all of the capsules studied, regardless of their geometry (Figure 3a). Importantly, the percentage of cells associated with AR1 capsules (~300 nm in diameter) was significantly greater than that observed for the higher aspect ratio (AR2, AR3, and AR4) capsules. This preferential cellular association with spherical capsules is more apparent after the first 6 h of incubation with cells. Consistent with this observation, the efficiency of cellular association with AR4 capsules was lower than AR2 and AR3 capsules for all of the time intervals examined (Figure 3a). For instance, after 24 h incubation, over 90% of cells were associated with the spherical capsules, around 60% of cells associated with AR2 and AR3 capsules, and about 40% of cells associated with AR4 capsules. As increasing the AR of the capsules will also increase the apparent capsule size, this differential cellular association for this series of capsules could also result from the change in volume.

To clarify the influence of size, we evaluated the cellular association of two additional spherical capsules, with diameters of 585 and 1100 nm (Figure 3b). The 585 nm-diameter capsules have a similar internal volume to the AR3 capsules, whereas the 1100 nm-diameter capsules possess a larger internal volume than the AR4 capsules, but a similar diameter to the long axis of the AR4 capsules. It was observed that

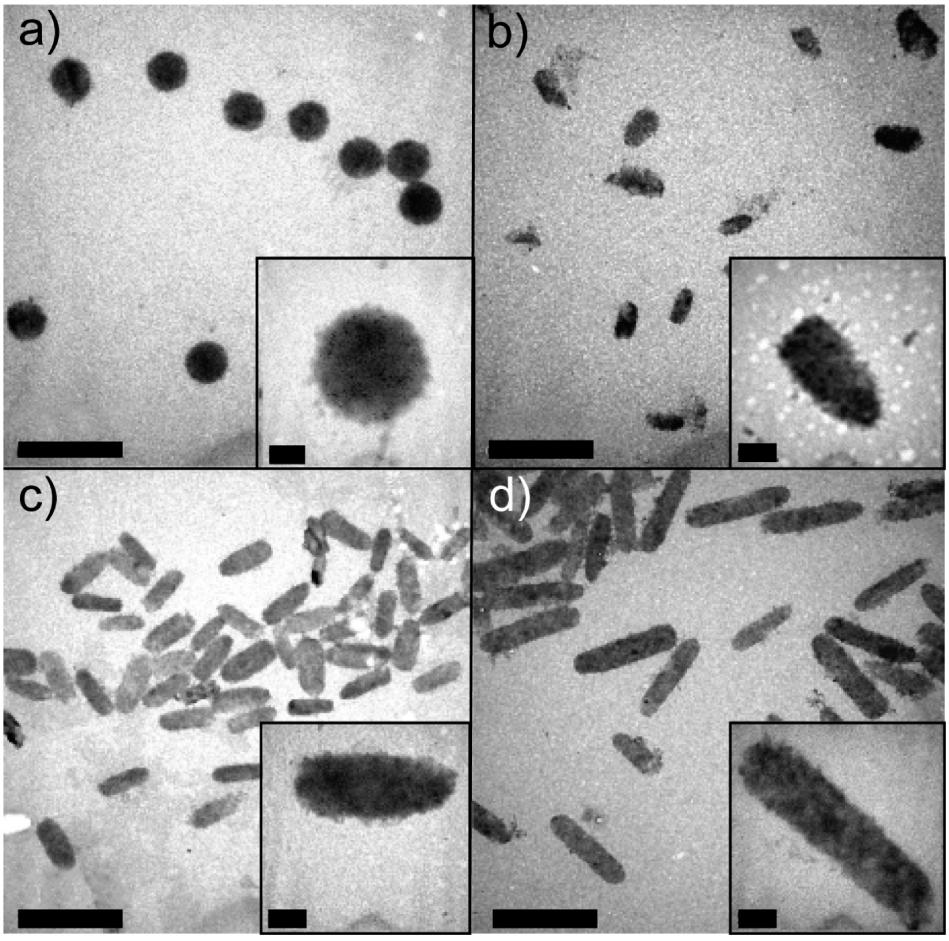


**Figure 1. TEM images of PMA HCs with aspect ratios of (a) AR1, (b) AR2, (c) AR3, and (d) AR4, obtained by using silica rod templates of AR1, AR2, AR3, and AR4, respectively. Scale bars are 2 $\mu$m. Scale bars in the insets are 0.2 $\mu$m.**

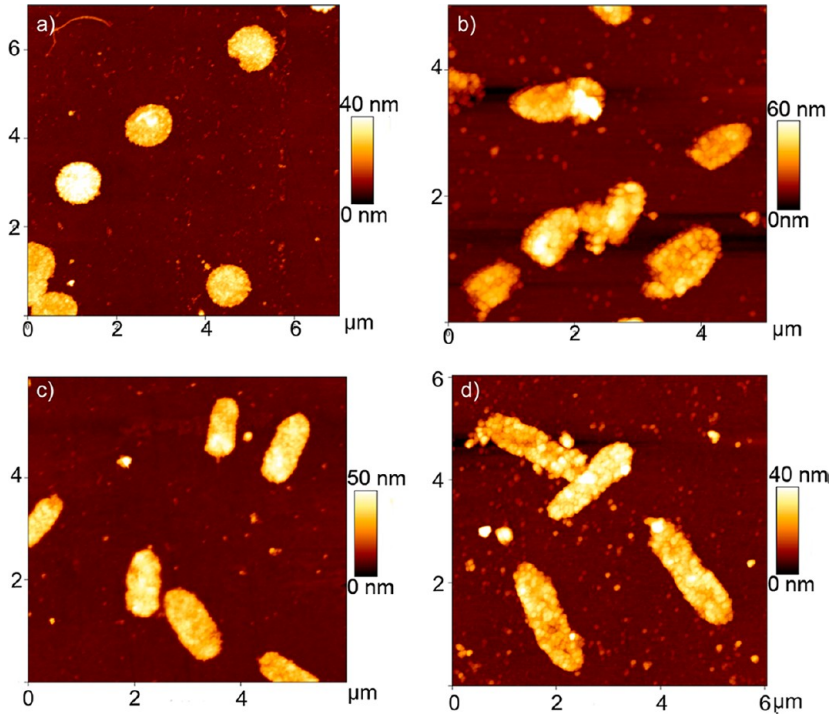


**Figure 2. AFM images of PMA HCs with various aspect ratios: (a) AR1; (b) AR2; (c) AR3; and (d) AR4.**

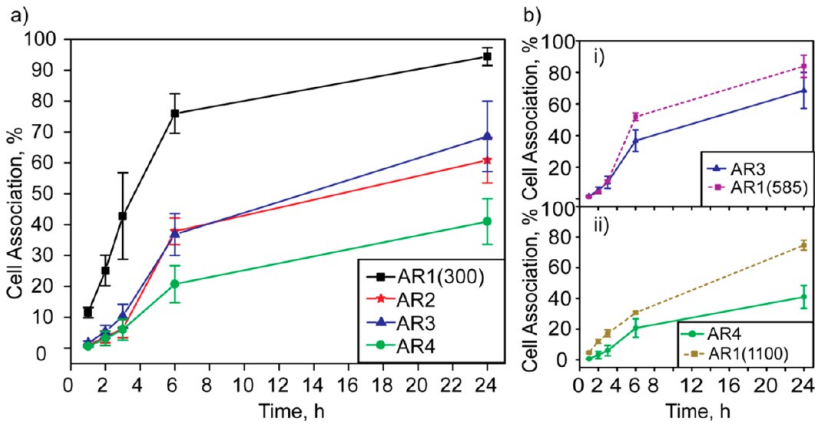


**Figure 3. Cellular association of AF633-labeled PMA HCs with HeLa cells over a 24 h incubation period. (a) Comparison of PMA capsules with various ARs. (b) Comparison between rod-shaped and spherical PMA capsules with similar volume (i) or similar major axis length (ii). Cells were incubated with PMA HCs for various intervals at 37 °C, 5% $CO_2$. The percentage of cells associated with capsules was quantified by flow cytometry. Data are the mean ± standard error of at least three independent experiments, and at least 20 000 cells were analyzed in each experiment.**

about 55% of cells associated with spherical 585 nm-diameter capsules after 6 h incubation, whereas about 35% of cells associated with AR3 rod-shaped capsules after the same time (Figure 3bi). A higher cellular association of spherical 585 nm-diameter capsules compared with AR3 capsules was also observed after 24 h (Figure 3bi). Moreover, spherical 1100 nm-diameter capsules also demonstrated significantly enhanced cellular association compared with AR4 capsules over the 24 h incubation period, even though the spherical capsules have a greater volume than the rod-shaped capsules (Figure 3bii). At 24 h, the spherical 1100 nm-diameter capsules showed almost a 2-fold greater cellular association than the AR4 capsules (Figure 3bii). Taken together, these data demonstrate that the cellular association is strongly dependent on PMA HC size and shape, with an increase in AR resulting in a decrease in cellular association. The dominant effect arising from AR (compared with the internal volume) on cellular association observed in this study, particularly for the AR4 and 1100 nm-diameter AR1 capsules, is in good agreement with a study on shape-switching poly(lactide-*co*-glycolide) particles,[36] suggesting that AR1 capsules have a higher probability of uptake in comparison to rod-shaped capsules.

Quantitative analysis of internalization of PMA HCs with various ARs was undertaken by using imaging flow cytometry, which captures bright-field and fluorescence images of cells simultaneously, allowing statistical and quantitative analysis of internalization on a large number of cells. HeLa cells were incubated with AF633-labeled PMA HCs with varying ARs for 6 h at 37 °C (5% $CO_2$) at a capsule-to-cell ratio of 100:1, trypsinized, and subsequently analyzed. On the basis of the spatial relationship between fluorescent capsules and bright-field images of cells, the internalization is measured using the built-in internalization function in the IDEAS software. A positive internalization factor correlates to cells with internalized capsules, whereas a negative factor corresponds to cells with surface-bound capsules. Hence, the higher percentage of cells with a positive internalization factor indicates a higher internalization probability for the cells associated with capsules. As shown in Figure 4, the percentage of cells with positive internalization factors decreases with an increase in the capsule AR, from 91.1% for AR1(300) capsules to 76.7% for AR4 capsules. This trend suggests that the capsules with higher ARs have a higher tendency of binding to the cell surface, rather than being internalized. To confirm that internalization is dependent on capsule shape, we examined the cellular internalization of AR1(585) and AR1(1100) capsules. Despite these two capsules showing different cellular association after 6 h incubation with cells (55% cells for AR1(585) and 20% cells for AR1(1100), respectively, Figure 3), the internalization probability for the cells associated with capsules was very similar, as the percentage of cells with positive internalization factors was 88.1% for AR1(585) and 87.1% for AR1(1100), respectively (Supporting Information, Figure S3). Taken together, the internalization analyses using imaging flow demonstrates a decrease in internalization probability with an increase in capsule AR, suggesting a slower uptake for rod-shaped capsules compared with spherical capsules. This is consistent with the findings of other studies that an increase in AR leads to an extended membrane wrapping time during cellular internalization.[37] The enhanced cell membrane retention of the AR4 capsules was also observed using fluorescence deconvolution microscopy. After treatment with the PMA HCs capsules (AR1 to AR4) for 6 h, the cell membrane was stained with AF488-WGA. Fluorescence deconvolution microscopy images showed that a proportion of AR4 capsules was bound on the cell membrane even after extensive washing with phosphate buffered saline (PBS)

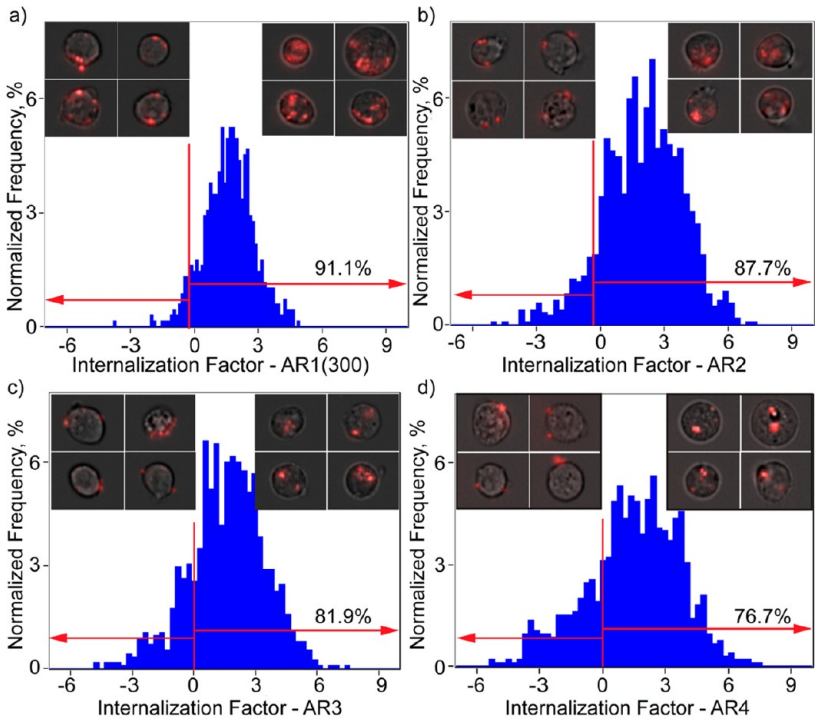


**Figure 4. Quantification of the internalization of AF633-labeled PMA HCs in HeLa cells by imaging flow cytometry. The cells were incubated with capsules at a capsule-to-cell ratio of 100:1 for 6 h at 37 °C, 5% $CO_2$. The degree of internalization is expressed as the internalization factor (IF). An overlay of the bright-field and fluorescence images of cells is shown (in the insets) for two representative areas: capsules bound with the cell membrane (negative IF) and capsules internalized within cells (positive IF).**

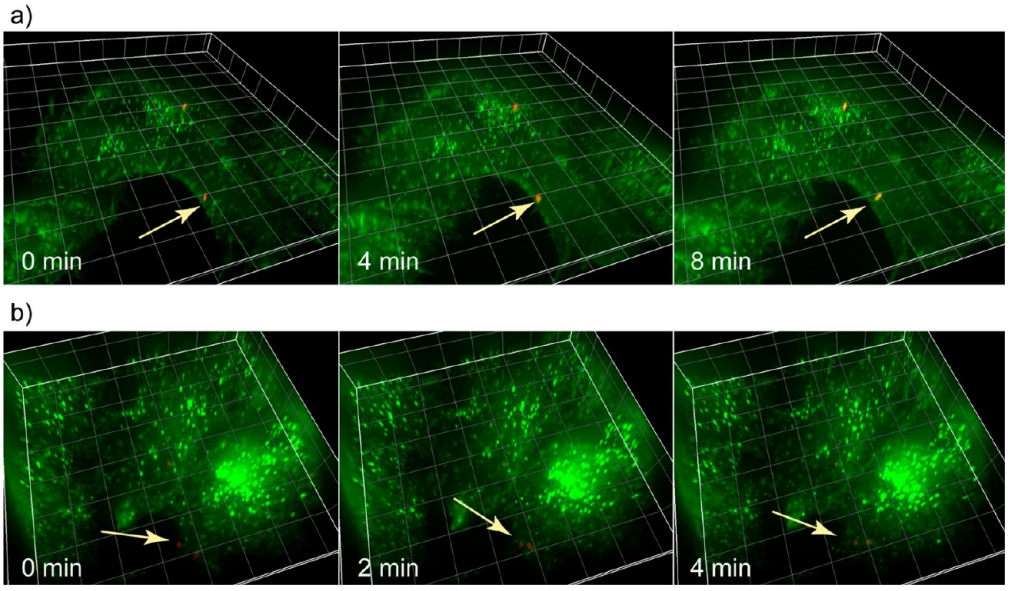


**Figure 5. Time lapse microscopy images of membrane-stained HeLa cells internalizing AF633-fluorescently labeled PMA HCs of (a) AR3 and (b) AR1(585). All cells were incubated with PMA HCs (red) for 30 min at 37 °C, 5% $CO_2$ followed by cell membrane staining with AF488 WGA for 7 min. The media was exchanged to $CO_2$-independent media and cells were then imaged using deconvolution microscopy. AR3 capsules were internalized after 8 min of engagement with the membrane, while AR1(585) capsules were internalized within 2 min after contact with the cell membrane. The grids are 10 $\mu$m × 10 $\mu$m.**

(Supporting Information, Figure S4d). In contrast, spherical capsules were effectively internalized, with a negligible number bound to the cell membrane (Supporting Information, Figure S4a), which is consistent with previous reports on the internalization of PMA HCs.[38]

To further investigate the influence of capsule shape on cell internalization, we acquired time lapse live cell images of cellular uptake of the capsules. HeLa cells were pulsed with AF633-labeled PMA HCs with varying ARs for 30 min at 37 °C (5% $CO_2$) at a capsule-to-cell

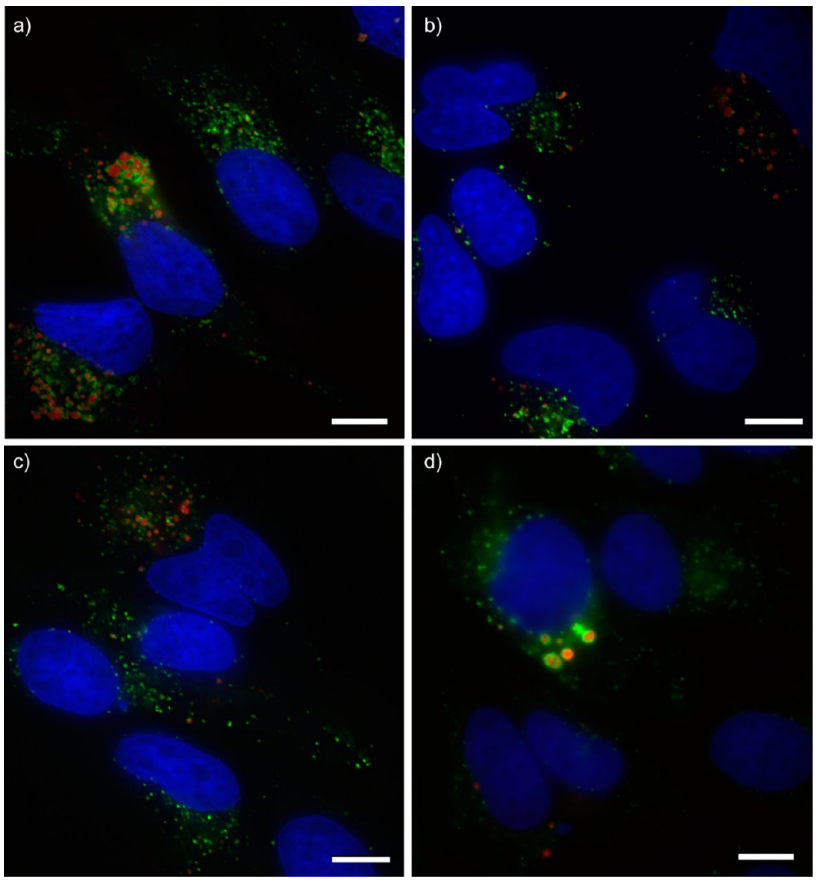


**Figure 6. Deconvolution microscopy images of the cellular fate of AF633-fluorescently labeled PMA HCs with different ARs inside HeLa cells: (a) AR1, (b) AR2, (c) AR3, and (d) AR4. The images are representative slices of cells. All cells were incubated with PMA HCs (red) for 24 h at 37 °C, 5% $CO_2$. PMA HCs are colocalized with late endosomes and lysosomes, which were immunostained with anti-LAMP1 antibody (green). Nuclei were counterstained with Hoechst 33342 (blue). Scale bars are 20 $\mu$m.**

ratio of 100:1 to allow the capsule−cell membrane interactions. Next, the cell membrane was stained with AF488-WGA and the internalization of individual capsules was recorded by time lapse imaging with 1 min intervals. We chose spherical 585 nm-diameter and AR3 PMA HCs, as those two capsules have a similar volume and are efficiently internalized (based on the flow cytometry analysis). AR3 capsules exhibited a prolonged retention on the cell surface and were internalized after 8 min (Figure 5a), while AR1(585) capsules demonstrated faster internalization, that is, the capsules were internalized into cells after 2 min from the moment of engagement with the cell membrane (Figure 5b). The different internalization efficiency between spherical and AR3 capsules was observed in at least three independent time lapse live cell experiments (an additional example is shown in Supporting Information, Figure S5). Several recent studies have reported that high AR particles show less efficient uptake than their spherical counterparts, which is attributed to the larger average radius of nonspherical particles experienced by cells during endocytosis.[16,38] Our data on the PMA HCs with various aspect ratios showed a negative correlation (Figure 3) between internalization rate and aspect ratio, given their identical surface chemistry.

The intracellular distribution of internalized capsules was further investigated by deconvolution fluorescence microscopy. Cells were incubated with AF633-labeled capsules at a capsule-to-cell ratio of 100:1 for 24 h. Following the treatment, the lysosomes in HeLa cells were identified by immunostaining with an antilysosome-associated membrane protein 1 (anti-LAMP1) antibody. As the lysosomes were stained green and the capsules were labeled red, the yellow staining indicates colocalization between lysosomes and capsules. As shown in Figure 6, the majority of internalized capsules are associated with LAMP1 positive compartments, suggesting that they are accumulated in lysosomes regardless of the ARs. It is notable that the AR4 capsules lost their original elongated shape when internalized (Figure 6d), which is consistent with previous reports on the deformation of polyelectrolyte capsules that occurs as a result of cell internalization.[38,39] The persistent lysosomal accumulation for the capsules with various ARs suggests that AR does not influence the intracellular fate of PMA HCs, but significantly impacts their internalization kinetics.

## CONCLUSIONS

We have reported the preparation of PMA HCs with tunable AR and have examined their association and internalization behavior with cells. PMA HCs were generated *via* LbL assembly through templating a series of silica particles with well-defined shape. The HCs retained the shape and AR of the templates, but their dimensions were enlarged compared with those of the templates due to swelling in aqueous solution. The PMA HC cellular association kinetics and internalization were quantitatively evaluated using flow cytometry and imaging flow cytometry, and revealed slower and less cellular internalization with increasing AR of the PMA HCs. Fluorescence microscopy analysis confirmed that the capsules with higher AR were more slowly internalized compared with the spherical capsules. Although the internalization kinetics varied with aspect ratio, lysosomal compartmentalization of the PMA HCs remained similar for all of the capsules, regardless of their shape, suggesting that shape plays a dominant role in determining the kinetics but not the intracellular fate. This study provides insights into the specific role of capsule AR on cellular processing, aiding in the development of LbL capsules for biological applications.

## METHODS

**Materials.** Poly(methacrylic acid, sodium salt) (PMA, $M_w$ 15 kDa) was purchased from Polysciences (USA). Poly(*N*-vinyl pyrrolidone) (PVPON, $M_w$ 10 and 40 kDa), *N*-(3-dimethylaminopropyl)-*N*′-ethylcarbodiimide (EDC), *N*-chloro-*p*-toluenesulfonamide sodium salt (chloramine T), hydrofluoric acid (HF), dithiothreitol (DTT), sodium citrate dihydrate, 1-pentanol, tetraethyl orthosilicate (TEOS), and phosphate-buffered saline were purchased from Sigma-Aldrich and used as received. 3-(*N*-Morpholino)propanesulfonic acid (MOPS) was obtained from Acros Organics. Sodium acetate (NaOAc), 2-(*N*-morpholino)-ethane-sulfonic acid (MES), and ammonia were purchased from Merck. Pyridine dithioethylamine hydrochloride (PDA-HCl) was obtained from Shanghai Speed Chemical Co. Ltd., China. Alexa Fluor 488 goat antimouse IgG, Alexa Fluor 488 C5 maleimide (AF488), and Alexa Fluor 633 C5 maleimide (AF633) reactive dyes were purchased from Invitrogen. $SiO_2$ particles of 296, 585, and 1100 nm-diameter were purchased from MicroParticles GmbH as a 5 wt % suspension and were used as received. Mouse antihuman LAMP1 monoclonal antibody (clone H4A3) was purchased from BD Pharmingen. Ultrapure water with resistance greater than 18 MΩ cm was obtained from an inline Millipore RiOs/Origin system (Millipore Corporation, USA).

**Preparation of Silica Rods.** Silica rods were prepared according to the protocol reported by Kuijk *et al.*[40] Briefly, 3 g of PVPON ($M_w$, 40 kDa) was dissolved in 30 mL of 1-pentanol overnight in a 50 mL plastic tube; 3.0 mL of absolute ethanol, 0.8 mL of Milli Q water, 0.2 mL of sodium citrate dihydrate solution (0.2 M in water), and 0.7 mL of ammonia (25 wt %) were then separately added to the mixture. The tube was hand shaken for 2 min to mix the contents, and 0.3 mL of TEOS was then added to the mixture. After shaking again for 2 min, the tube was kept static and the reaction was allowed to proceed at ambient temperature for different time intervals. Rods with an AR of 2, 3, and 4 were prepared by using a reaction time of 1, 1.5, and 3.5 h, respectively. To purify the rods produced, the reaction mixture was centrifuged at 3000*g* for 30 min. The pellet was separately washed twice with ethanol, twice with water, and finally dispersed in ethanol. To improve monodispersity, the rods were further purified through multistep gravity sedimentation. In this process, the rods were suspended in ethanol with a concentration of ∼0.5 wt % in a 50 mL centrifugation tube. After standing the tube vertical for different lengths of time, the middle part of the suspension in the tube was collected. The time used depends on the length of the rods. For example, to purify the 2 $\mu$m-long rods, the suspension was kept static for ∼4 h, while for the shortest rods, the suspension was kept static overnight before collecting the rods.

**Preparation of Thiolated PMA ($PMA_{SH}$).** Poly(methacrylic acid) was modified with 9% thiol groups by using pyridine dithioethylamine hydrochloride (PDA-HCl) *via* carbodiimide coupling, as described elsewhere.[41]

**Assembly of Rodlike PMA HCs.** PMA HCs with AR1 were templated from commercially available spherical silica particles with a diameter of 296 nm, as described previously.[41] Rodlike PMA HCs were prepared with a similar protocol; however, a few variations were incorporated. In particular, a suspension of the $SiO_2$ particles (5 wt %) was rinsed and redispersed in NaOAc buffer (50 mM, pH 4) using vortexing and sonication (1 min each) in siliconized tubes three times. After the third wash the particles were redispersed at a concentration of 10 wt %. An equal volume of PVPON solution (4 g $L^{-1}$) in NaOAc buffer (50 mM, pH 4) was then added and the resulting suspension was incubated for 10 min with constant shaking to effect polymer adsorption. The sample was then washed (three times) and redispersed (vortexing and sonication for 1 min) in NaOAc buffer (50 mM, pH 4). Four g $L^{-1}$ of $PMA_{SH}$ solution in NaOAc buffer (50 mM, pH 4) was then added to the 10 wt % particle suspension in acetate buffer and incubated for another 10 min. The adsorption of the two polymers describes the assembly of a single bilayer. The process was repeated until four bilayers were deposited. The multilayered polymer film was then stabilized using thiol−disulfide chemistry. Disulfide-stabilized capsules were obtained by treating the capsule suspension with 2.8 mM of chloramine T solution in MES buffer (50 mM, pH 6) for 1 min, followed by two washing steps with MES buffer (50 mM, pH 6) and redispersion in NaOAc buffer (50 mM, pH 4). Fluorescently labeled core−shell particles were obtained by mixing the particles with 0.1 g $L^{-1}$ of AF488 or AF633 maleimide solution in MES buffer (50 mM, pH 6) overnight. The fluorescent particles were washed (twice) with MES buffer (50 mM, pH 6) and redispersed in pH 4 buffer.

Capsules were obtained by dissolving the silica templates using 5 M hydrofluoric acid (HF) for 2 min, followed by at least four washing/redispersion cycles (4500*g*, 5 min, vortexing only) with NaOAc buffer (50 mM, pH 4). (*Caution! Hydrofluoric acid is highly toxic and great care must be taken when handling it*).

Capsule counting was performed using a CyFlow Space (Partec GmbH) flow cytometer using lasers with excitation wavelengths of 488 and 633 nm. The counting procedure is described elsewhere.[31] Briefly, a small aliquot of AF633-fluorescently labeled PMA HCs dispersed in PBS was mixed with a similar volume of AF488-fluorescently labeled PVPON in NaOAc buffer (100 mM, pH 4, 1 g $L^{-1}$), which was synthesized by reversible addition−fragmentation chain transfer (RAFT) polymerization and one of the end-groups was modified to contain AF488.[30] The capsule dispersion was left for 5 min to allow for AF488-labeled PVPON to adsorb on the surface of the capsules, and then 1 $\mu$L of the dispersion was diluted in NaOAc buffer (20 mM, pH 4) for flow cytometry analysis. The flow cytometer triggered on AF488 fluorescence, counting the number of capsules in the known volume. The initial capsule concentration was back calculated on the basis of the known dilution.

**Cell Cultures.** HeLa cells were maintained in Dulbecco's modified Eagle's medium (DMEM) media (Gibco) with the addition of

2 mM L-glutamine and 10% fetal bovine serum at 37 °C in a 5% $CO_2$ humidified atmosphere and subcultured prior to confluence using trypsin.

**Cellular Association Analysis.** HeLa cells were plated at a density of $1 \times 10^5$ cells per well into 24-well plates and allowed to adhere overnight. Cells were then incubated with AF633-labeled PMA HCs with various ARs at a capsule-to-cell ratio of 100:1 for different time intervals (37 °C, 5% $CO_2$) individually. These include AR1 (templated from 296 nm-, 585 nm-, and 1100 nm-diameter spherical particles), AR2 (360 nm × 700 nm), AR3 (410 nm × 1120 nm) and AR4 (340 nm × 1290 nm) capsules. After the treatment, the cells were washed with PBS three times and harvested by trypsinization and centrifugation at 400*g* for 5 min. The cell pellet was resuspended in PBS and analyzed by flow cytometry. Flow cytometry analysis was performed using a CyFlow Space (Partec GmbH) flow cytometer using lasers with excitation wavelengths of 488 and 633 nm. In each measurement at least 20 000 cells were analyzed.

**Internalization Analysis by Imaging Flow Cytometry.** Samples were prepared as described above. Briefly, $5 \times 10^5$ cells were plated to 6-well plates and treated with AF633-labeled PMA HCs at a capsule-to-cell ratio of 100:1 for 6 h. Images of 10 000 cells and the capsule fluorescence intensities were acquired. The internalization analysis was performed using the built-in internalization feature of IDEAS software on single cells associated with capsules.

**Cell Imaging.** HeLa cells were plated at $3 \times 10^4$ cells per well into 8-well Lab-Tek I chambered coverglass slides (Thermo Fisher Scientific, Rochester) and allowed to adhere overnight. Cells were then incubated with AF633-labeled PMA HCs with ARs from 1 to 4 at a capsule-to cell ratio of 100:1 for 24 h (37 °C, 5% $CO_2$) individually. Following this, cells were washed with PBS three times and fixed with 4% paraformaldehyde for 30 min at room temperature.

Membrane staining of the cells was carried out by incubating them with Alexa Fluor 488 Wheat Germ Agglutinin (AF488-WGA, 5 $\mu$g mL$^{-1}$) at room temperature for 30 min. Late endosomes and lysosomes were immunostained with anti-LAMP1 antibody (2.5 $\mu$g mL$^{-1}$) and AF488-goat antimouse IgG (2 $\mu$g mL$^{-1}$). Nuclei were counterstained with Hoechst 33342 (2 $\mu$g mL$^{-1}$). Fluorescence images and optical sections were collected using a deconvolution fluorescence (DeltaVision, Applied Precision) microscope equipped with a 60× 1.42 NA oil objective with a standard FITC/CY5 filter set. Images were processed with Imaris 6.3.1 (Bitplane) using the maximum intensity projection.

**Live Cell Time Lapse Imaging.** HeLa cells were plated at $2 \times 10^4$ cells per well into 8-well Lab-Tek I chambered coverglass slides (Thermo Fisher Scientific, Rochester) and allowed to adhere overnight. Cells were then incubated with AF633-labeled PMA HCs with ARs from 1 to 4 at a capsule-to-cell ratio of 100:1 for 30 min (37 °C, 5% $CO_2$) individually. AF488-WGA (5 $\mu$g mL$^{-1}$) was added for 7 min (37 °C, 5% $CO_2$) to stain the cell membrane. Subsequently, the media was removed and replaced by fresh $CO_2$-independent media (Gibco) with the addition of 10% GlutaMax and 10% fetal bovine serum. Time lapse fluorescence images and optical sections were collected using fluorescence deconvolution microscopy for 1 h. The acquired movies were processed with Imaris 6.3.1 software (Bitplane).

**Methods.** TEM images were taken using a Philips CM120 BioTWIN electron microscope operated at 120 kV. All TEM grids were plasma treated for 10 s prior to use. Five $\mu$L of the capsule dispersion was placed onto a carbon-coated Formvar film mounted on 300-mesh copper grids (ProSciTech, Australia) for 5 min and the grids were blotted dry using filter paper.

AFM scans were carried out with an MFP-3D Asylum Research instrument in AC mode using ultrasharp SiN gold-coated cantilevers (NT-MDT). Five $\mu$L of the capsule dispersion in Milli Q water was deposited onto glass slides pretreated with poly-(ethyleneimine) (PEI).

*Conflict of Interest:* The authors declare no competing financial interest.

*Acknowledgment.* This work was supported by the Australian Research Council under the Australian Laureate Fellowship (F.C.), Federation Fellowship (F.C.), and Discovery Project (F.C.) schemes, and by the National Health and Medical Research Council (NHMRC) Program Grant 487922 (F.C.). James P. Best is acknowledged for helpful discussions on preparation of the manuscript. Kang Liang is acknowledged for assistance with the AFM measurements.

*Supporting Information Available:* TEM images of rod-shaped silica particles, height profile of AR3 PMA capsules measured by AFM, quantitative internalization analysis of AR1-(585) and AR1(1100) capsules, fluorescence deconvolution microscopy images of the internalized PMA HCs and time lapse microscopy images of the internalization of AR1(585) and AR3 PMA HCs. This material is available free of charge *via* the Internet at http://pubs.acs.org.

## REFERENCES AND NOTES

1. Torchilin, V. Micellar Nanocarriers: Pharmaceutical Perspectives. *Pharm. Res.* **2007**, *24*, 1–16.
2. Discher, D. E.; Ahmed, F. Polymersomes. *Annu. Rev. Biomed. Eng.* **2006**, *8*, 323–341.
3. Kataoka, K.; Harada, A.; Nagasaki, Y. Block Copolymer Micelles for Drug Delivery: Design, Characterization and Biological Significance. *Adv. Drug Delivery Rev.* **2001**, *47*, 113–131.
4. Becker, A. L.; Johnston, A. P. R.; Caruso, F. Layer-By-Layer-Assembled Capsules and Films for Therapeutic Delivery. *Small* **2010**, *6*, 1836–1852.
5. Ariga, K.; Lvov, Y. M.; Kawakami, K.; Ji, Q.; Hill, J. P. Layer-by-Layer Self-Assembled Shells for Drug Delivery. *Adv. Drug Delivery Rev.* **2011**, *63*, 762–771.
6. Cortez, C.; Tomaskovic-Crook, E.; Johnston, A. P. R.; Scott, A. M.; Nice, E. C.; Heath, J. K.; Caruso, F. Influence of Size, Surface, Cell Line, and Kinetic Properties on the Specific Binding of A33 Antigen-Targeted Multilayered Particles and Capsules to Colorectal Cancer Cells. *ACS Nano* **2007**, *1*, 93–102.
7. Schipper, M. L.; Iyer, G.; Koh, A. L.; Cheng, Z.; Ebenstein, Y.; Aharoni, A.; Keren, S.; Bentolila, L. A.; Li, J.; Rao, J.; *et al.* Particle Size, Surface Coating, and PEGylation Influence the Biodistribution of Quantum Dots in Living Mice. *Small* **2009**, *5*, 126–134.
8. Howard, M. D.; Jay, M.; Dziubla, T. D.; Lu, X. PEGylation of Nanocarrier Drug Delivery Systems: State of the Art. *J. Biomed. Nanotechnol.* **2008**, *4*, 133–148.
9. Byrne, J. D.; Betancourt, T.; Brannon-Peppas, L. Active Targeting Schemes for Nanoparticle Systems in Cancer Therapeutics. *Adv. Drug Delivery Rev.* **2008**, *60*, 1615–1626.
10. Doshi, N.; Mitragotri, S. Designer Biomaterials for Nanomedicine. *Adv. Funct. Mater.* **2009**, *19*, 3843–3854.
11. Petros, R. A.; DeSimone, J. M. Strategies in the Design of Nanoparticles for Therapeutic Applications. *Nat. Rev. Drug Discovery* **2010**, *9*, 615–627.
12. Geng, Y.; Dalhaimer, P.; Cai, S.; Tsai, R.; Tewari, M.; Minko, T.; Discher, D. E. Shape Effects of Filaments *versus* Spherical Particles in Flow and Drug Delivery. *Nat. Nanotechnol.* **2007**, *2*, 249–255.
13. Perry, J. L.; Herlihy, K. P.; Napier, M. E.; DeSimone, J. M. PRINT: A Novel Platform Toward Shape and Size Specific Nanoparticle Theranostics. *Acc. Chem. Res.* **2011**, *44*, 990–998.
14. Chauhan, V. P.; Popović, Z.; Chen, O.; Cui, J.; Fukumura, D.; Bawendi, M. G.; Jain, R. K. Fluorescent Nanorods and Nanospheres for Real-Time *in Vivo* Probing of Nanoparticle Shape-Dependent Tumor Penetration. *Angew. Chem., Int. Ed.* **2011**, *50*, 11417–11420.
15. Chithrani, B. D.; Ghazani, A. A.; Chan, W. C. W. Determining the Size and Shape Dependence of Gold Nanoparticle Uptake into Mammalian Cells. *Nano Lett.* **2006**, *6*, 662–668.
16. Yoo, J.-W.; Doshi, N.; Mitragotri, S. Endocytosis and Intracellular Distribution of PLGA Particles in Endothelial Cells: Effect of Particle Geometry. *Macromol. Rapid Commun.* **2010**, *31*, 142–148.

17. Meng, H.; Yang, S.; Li, Z.; Xia, T.; Chen, J.; Ji, Z.; Zhang, H.; Wang, X.; Lin, S.; Huang, C.; *et al*. Aspect Ratio Determines the Quantity of Mesoporous Silica Nanoparticle Uptake by a Small GTPase-Dependent Macropinocytosis Mechanism. *ACS Nano* **2011**, *5*, 4434–4447.
18. Gratton, S. E. A.; Ropp, P. A.; Pohlhaus, P. D.; Luft, J. C.; Madden, V. J.; Napier, M. E.; DeSimone, J. M. The Effect of Particle Design on Cellular Internalization Pathways. *Proc. Natl. Acad. Sci. U.S.A.* **2008**, *105*, 11613–11618.
19. Caruso, F.; Caruso, R. A.; Möhwald, H. Nanoengineering of Inorganic and Hybrid Hollow Spheres by Colloidal Templating. *Science* **1998**, *282*, 1111–1114.
20. Donath, E.; Sukhorukov, G. B.; Caruso, F.; Davis, S. A.; Möhwald, H. Novel Hollow Polymer Shells by Colloid-Templated Assembly of Polyelectrolytes. *Angew. Chem., Int. Ed.* **1998**, *37*, 2201–2205.
21. Artyukhin, A. B.; Bakajin, O.; Stroeve, P.; Noy, A. Layer-by-Layer Electrostatic Self-Assembly of Polyelectrolyte Nanoshells on Individual Carbon Nanotube Templates. *Langmuir* **2004**, *20*, 1442–1448.
22. Mayya, K. S.; Gittins, D. I.; Dibaj, A. M.; Caruso, F. Nanotubes Prepared by Templating Sacrificial Nickel Nanorods. *Nano Lett.* **2001**, *1*, 727–730.
23. Mueller, R.; Daehne, L.; Fery, A. Hollow Polyelectrolyte Multilayer Tubes: Mechanical Properties and Shape Changes. *J. Phys. Chem. B* **2007**, *111*, 8547–8553.
24. Müller, K.; Quinn, J. F.; Johnston, A. P. R.; Becker, M.; Greiner, A.; Caruso, F. Polyelectrolyte Functionalization of Electrospun Fibers. *Chem. Mater.* **2006**, *18*, 2397–2403.
25. Neu, B.; Voigt, A.; Mitlöhner, R.; Leporatti, S.; Gao, C. Y.; Donath, E.; Kiesewetter, H.; Möhwald, H.; Meiselman, H. J.; Bäumler, H. Biological Cells as Templates for Hollow Microcapsules. *J. Microencapsulation* **2001**, *18*, 385–395.
26. Garbers, E.; Mitlöhner, R.; Georgieva, R.; Bäumler, H. Activity of Immobilized Trypsin in the Layer Structure of Polyelectrolyte Microcapsules (PEMC). *Macromol. Biosci.* **2007**, *7*, 1243–1249.
27. Caruso, F.; Trau, D.; Möhwald, H.; Renneberg, R. Enzyme Encapsulation in Layer-by-Layer Engineered Polymer Multilayer Capsules. *Langmuir* **2000**, *16*, 1485–1488.
28. Sivakumar, S.; Gupta, J. K.; Abbott, N. L.; Caruso, F. Monodisperse Emulsions through Templating Polyelectrolyte Multilayer Capsules. *Chem. Mater.* **2008**, *20*, 2063–2065.
29. Zelikin, A. N.; Price, A. D.; Städler, B. Poly(Methacrylic Acid) Polymer Hydrogel Capsules: Drug Carriers, Sub-compartmentalized Microreactors, Artificial Organelles. *Small* **2010**, *6*, 2201–2207.
30. Shimoni, O.; Postma, A.; Yan, Y.; Scott, A. M.; Heath, J. K.; Nice, E. C.; Zelikin, A. N.; Caruso, F. Macromolecule Functionalization of Disulfide-Bonded Polymer Hydrogel Capsules and Cancer Cell Targeting. *ACS Nano* **2012**, *6*, 1463–1472.
31. Zelikin, A. N.; Breheney, K.; Robert, R.; Tjipto, E.; Wark, K. Cytotoxicity and Internalization of Polymer Hydrogel Capsules by Mammalian Cells. *Biomacromolecules* **2010**, *11*, 2123–2129.
32. De Rose, R.; Zelikin, A. N.; Johnston, A. P. R.; Sexton, A.; Chong, S. F.; Cortez, C.; Mulholland, W.; Caruso, F.; Kent, S. J. Binding, Internalization, and Antigen Presentation of Vaccine-Loaded Nanoengineered Capsules in Blood. *Adv. Mater.* **2008**, *20*, 4698–4703.
33. Yan, Y.; Wang, Y.; Heath, J. K.; Nice, E. C.; Caruso, F. Cellular Association and Cargo Release of Redox-Responsive Polymer Capsules Mediated by Exofacial Thiols. *Adv. Mater.* **2011**, *23*, 3916–3921.
34. Zelikin, A. N.; Li, Q.; Caruso, F. Disulfide-Stabilized Poly(methacrylic acid) Capsules: Formation, Cross-Linking, and Degradation Behavior. *Chem. Mater.* **2008**, *20*, 2655–2661.
35. Becker, A. L.; Zelikin, A. N.; Johnston, A. P. R.; Caruso, F. Tuning the Formation and Degradation of Layer-by-Layer Assembled Polymer Hydrogel Microcapsules. *Langmuir* **2009**, *25*, 14079–14085.
36. Yoo, J. W.; Mitragotri, S. Polymer Particles That Switch Shape in Response to a Stimulus. *Proc. Natl. Acad. Sci. U.S.A.* **2010**, *107*, 11205–11210.
37. Florez, L.; Herrmann, C.; Cramer, J. M.; Hauser, C. P.; Koynov, K.; Landfester, K.; Crespy, D.; Mailänder, V. How Shape Influences Uptake: Interactions of Anisotropic Polymer Nanoparticles and Human Mesenchymal Stem Cells. *Small* **2012**, *8*, 2222–2230.
38. Yan, Y.; Johnston, A. P. R.; Dodds, S. J.; Kamphuis, M. M. J.; Ferguson, C.; Parton, R. G.; Nice, E. C.; Heath, J. K.; Caruso, F. Uptake and Intracellular Fate of Disulfide-Bonded Polymer Hydrogel Capsules for Doxorubicin Delivery to Colorectal Cancer Cells. *ACS Nano* **2010**, *4*, 2928–2936.
39. Muñoz Javier, A.; Kreft, O.; Semmling, M.; Kempter, S.; Skirtach, A. G.; Bruns, O. T.; del Pino, P.; Bedard, M. F.; Rädler, J.; Käs, J.; *et al*. Uptake of Colloidal Polyelectrolyte-Coated Particles and Polyelectrolyte Multilayer Capsules by Living Cells. *Adv. Mater.* **2008**, *20*, 4281–4287.
40. Kuijk, A.; van Blaaderen, A.; Imhof, A. Synthesis of Monodisperse, Rodlike Silica Colloids with Tunable Aspect Ratio. *J. Am. Chem. Soc.* **2011**, *133*, 2346–2349.
41. Kulygin, O.; Price, A. D.; Chong, S. F.; Städler, B.; Zelikin, A. N.; Caruso, F. Subcompartmentalized Polymer Hydrogel Capsules with Selectively Degradable Carriers and Subunits. *Small* **2010**, *6*, 1558–1564.